RSC Advances

PAPER

View Article Online
View Journal | View Issue

Cite this: *RSC Adv.*, 2020, **10**, 39049

Impact of benzannulation on ESIPT in 2-(2′-hydroxyphenyl)-oxazoles: a unified perspective in terms of excited-state aromaticity and intramolecular charge transfer†

Leandro D. Mena, *[a] D. M. A. Vera[b] and María T. Baumgartner *[a]

Hydroxyphenyl-azoles are among the most popular ESIPT (Excited State Intramolecular Proton Transfer) scaffolds and as such, they have been thoroughly studied. Nevertheless, some aspects regarding the interplay between the emissive properties of these fluorophores and the size of their π-conjugated framework remain controversial. Previous studies have demonstrated that benzannulation of 2′-hydroxyphenyl-oxazole at the phenol group of the molecule can lead to either red- or blue-shifted fluorescence emission, depending on the site where it occurs. In this report, benzannulation at the heterocyclic unit (the oxazole site) is analysed in order to get the whole picture. The extension of π-conjugation does not significantly affect the ESIPT emission wavelength, but it leads instead to higher energy barriers for proton transfer in the first excited singlet state, as a consequence of dramatic changes in the charge transfer character of excitation caused by successive benzannulation. Theoretical calculations revealed an interesting connection between intramolecular charge transfer and excited-state aromaticity in the S_1 state. The theoretical approach presented herein allows the behaviour of hydroxyphenyl-oxazoles in the excited state to be rationalized and, more generally, a deeper understanding of the factors governing the ESIPT process to be obtained, a crucial point in the design of new and efficient fluorophores.

Received 3rd July 2020
Accepted 14th October 2020

DOI: 10.1039/d0ra05802e

rsc.li/rsc-advances

Introduction

The design of organic fluorophores with a π-conjugated system has become a fundamental part in the development of functional materials such as photovoltaic devices[1] and organic light-emitting diodes (OLEDs).[2] In this context, it is highly desirable to obtain red-shifted emission with large Stokes shifts, in order to minimize self-absorption effects and to obtain low signal-to-noise ratios for bioimaging applications.[3] Emitters based on ESIPT (Excited State Intramolecular Proton Transfer) have emerged as an interesting class of fluorophores since their emission usually occurs with anomalously high Stokes shifts (6000–12 000 cm^{-1}). As the ESIPT process is essentially an excited-state tautomerization, the keto tautomer formed upon photoexcitation (K*) is structurally different from the starting enol form (E), which causes the former to exhibit red-shifted fluorescence emission. In some cases, it is also possible to obtain dual fluorescence from both enol and keto forms, a unique feature that has been applied to the development of white light-emitting materials.[4] Additionally, ESIPT compounds present intense solid-state emission, a significant advantage over common fluorophores which usually undergo aggregation-induced fluorescence quenching in films or crystals.[5]

It is well known that, together with the introduction of electron donor and acceptor groups into the structure of a chromophore,[6] the modification of π-conjugation is the most common way to tune the absorption energy. In general, extending conjugation results in bathochromic shifts in absorption. Although the same is true for fluorescence in many systems,[7] this rule of thumb does not always apply for molecules that undergo significant structural changes in excited state. A particular example of this is the case of ESIPT fluorophores. Despite the excited state behaviour of this kind of molecules has been extensively studied, the influence of the conjugation extension on fluorescence emission remained controversial during the last decades.

Hydroxyphenyl-azoles represent an archetypical family of ESIPT fluorophores, among which 2-(2′-hydroxyphenyl)-benzoxazole (**HBO**, Scheme 1) is maybe one of the most studied.[8] In 1999, Nagaoka *et al.* were pioneers in suggesting that ESIPT emission of **HBO** depends on the size of the π-system

[a]*INFIQC, Departamento de Química Orgánica, Facultad de Ciencias Químicas, Universidad Nacional de Córdoba, Ciudad Universitaria, Córdoba, X5000HUA, Argentina. E-mail: lmena@fcq.unc.edu.ar; tere@fcq.unc.edu.ar*

[b]*QUIAMM-INBIOTEC-Departamento de Química, Facultad de Ciencias Exactas y Naturales, Universidad Nacional de Mar del Plata, Mar del Plata, Argentina*

† Electronic supplementary information (ESI) available. See DOI: 10.1039/d0ra05802e

of the phenol part of the molecule.[9] The authors interpreted the experimental results based on the "nodal plane model", a qualitative method according to which the ESIPT behaviour can be rationalised by considering the nodal plane of the wavefunction in excited state.[10] As a proof-of-concept, they studied two hydroxynaphthyl derivatives of **HBO** bearing 1-naphthol and 2-naphthol units, **1H2NBO** and **2H3NBO** (Scheme 1), and demonstrated that the emissive properties of both dyes were actually very different: the emission maxima of **1H2NBO** is at 470 nm in hexane, whereas **2H3NBO** shows ESIPT emission at 670 nm. In their report, the authors suggested that an effective red shift in emission can take place only if the extension of conjugation occurs along the nodal plane of the wavefunction in excited state, since in that way the keto tautomer becomes specially stabilized.

Ten years after Nagaoka's seminal work, the Arai group reported the ESIPT behaviour of 2-(2′-hydroxynaphthalenyl)-benzoxazole (**2H1NBO**, Scheme 1), another benzannulated derivative of **HBO** displaying unusually small Stokes shift.[11] The authors then expanded the investigation toward other naphthalene-fused 2-(2′-hydroxyaryl)benzazoles, finding that ESIPT emission of these dyes was blue-shifted compared to the model compound **HBO**, but without proposing a possible explanation for this effect.[12] Almost another ten years later, this unconventional behaviour has been revisited by different authors[13,14] under the light of the Baird's rule.[15] This rule, according to which $[4n + 2]$ π-aromatic annulenes become antiaromatic in the ππ* S_1 or T_1 state, has been successfully applied to rationalize the ESIPT emission profile of different benzannulated **HBO** derivatives by connecting the relative stability of the tautomers to their aromatic (antiaromatic) character in the ground (excited) state.

To the best of our knowledge, these antecedents only deal with the benzannulation of the phenol unit of **HBO**, that is, the donor part of the molecule. Nevertheless, the effects that benzannulation at the acceptor unit causes on ESIPT still remain unknown. Considering that the study of both the donor and the acceptor moieties of an ESIPT molecule is essential to get a complete understanding of the phenomenon, we present herein a thorough analysis aimed to clarify the impact that an increase in the π-conjugation of the oxazole unit in **HBO** has on the ESIPT process. Experimental results demonstrate that benzannulation does not necessarily lead to a significant red-shifted keto emission. In addition, DFT and TDDFT calculations enabled us to provide a reasonable explanation for the observed behaviour and to get deeper insights into the ESIPT reactivity of the studied system. Finally, a global comparison with previous results is proposed, revisiting the behaviour of the ring-fused phenol derivatives under the light of the Baird's and Clar's rules.

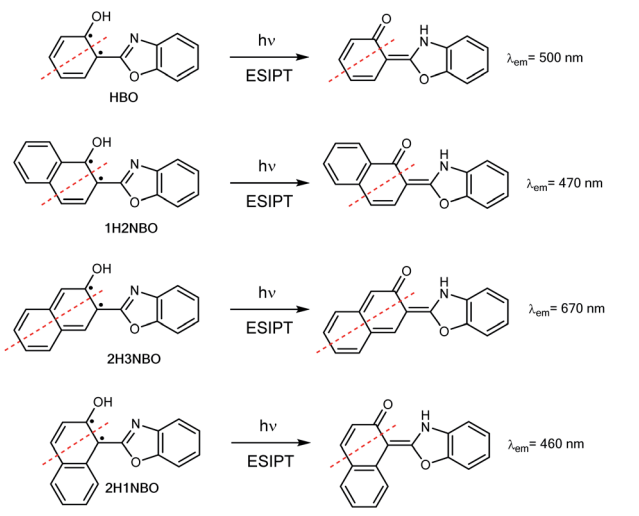

Scheme 1 ESIPT in HBO and its benzannulated derivatives 2-(1′-hydroxy-2′-naphthyl)-benzoxazole **1H2NBO**, 2-(2′-hydroxy-3-naphthyl)-benzoxazole **2H3NBO** and 2-(2′-hydroxy-1-naphthyl)-benzoxazole **2H1NBO**. Red broken lines indicate the nodal plane orthogonal to the molecular plane; dots indicate lone π electrons.

Results and discussion

To begin with the study, we propose a comparison between the ESIPT reaction in three azoles with heterocyclic systems of different length: 2-(2′-hydroxyphenyl)-oxazole (**HPO**), 2-(2′-hydroxyphenyl)-benzoxazole (**HBO**) and 2-(2′-hydroxyphenyl)-naphthoxazole (**HNO**) (Scheme 2). For this purpose, we have synthesized and characterized **HNO**, since the data available in literature about him was scarce. Throughout this text, the experimental data measured for **HNO** is contrasted to the data extracted from literature about **HBO** and **HPO**. Computational results presented herein regarding the three compounds were entirely calculated by us.

Spectroscopic properties

The UV-vis absorption spectra of **HPO** exhibit an $S_0 \rightarrow S_1$ (ππ*) transition with a maximum around 306–310 nm in different solvents according to literature,[16] whereas the maximum

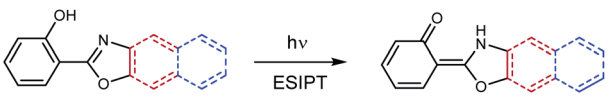

Scheme 2 ESIPT reaction in HPO and its benzannulated derivatives, HBO (red) and HNO (blue).

Table 1 Experimental UV-vis absorption and emission maxima for each compound in nm[h]

Dye	λ_{max} absorption (enol form)	λ_{max} emission (enol and keto forms)	
		λ_{enol}	λ_{keto}
HPO*	306[a], 306[b], 309[c]	340[g], 345[a], 345[b]	480[g], 460[a], 465[b]
HBO*	330[d], 334[c], 333[e]	362[c], 365[d], 351[b]	500[c], 474[d], 485[b]
HNO	343[f], 342[e], 342[d]	415[b], 430[d]	493[c], 483[d], 493[b]

[a] Ethanol. [b] Acetonitrile. [c] Hexane. [d] Methanol. [e] Dichloromethane. [f] Cyclohexane. [g] Methylcyclohexane. [h] *Data extracted from ref. 16 for **HPO** and from ref. 8*d* and *i* for **HBO**.

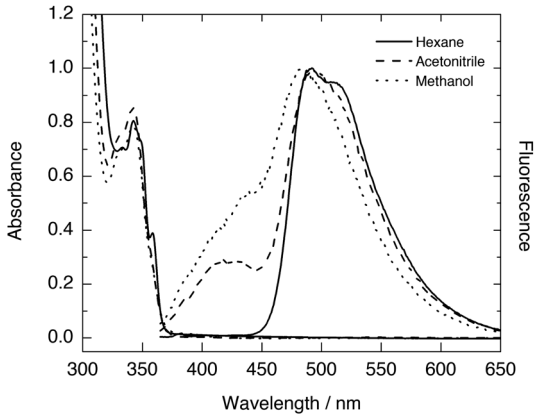

Fig. 1 UV-vis absorption and normalised fluorescence spectra of **HNO** in various solvents.

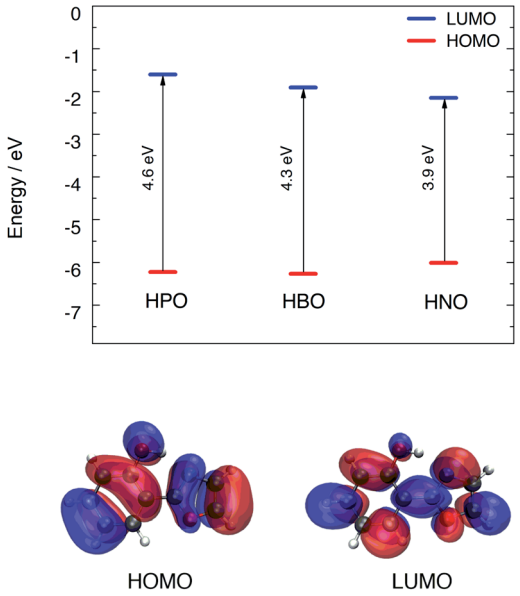

Fig. 2 Top: HOMO–LUMO energy levels for the three compounds calculated with B3LYP/6-31+G(d) in acetonitrile. Bottom: HOMO and LUMO distribution for **HPO**.

absorption reported for the same transition in **HBO** is located around 330–334 nm (Table 1).[8] This maximum is slightly red shifted (at 342–343 nm) in the case of **HNO** (Fig. 1). Clearly, the extension of conjugation leads to bathochromically shifted absorption, irrespective of the solvent employed.

The fluorescence emission spectra of **HPO** and **HBO** available in literature present dominant K* emission in non-polar environments, and dual emission from E* and K* forms in polar solvents such as methanol or acetonitrile (Table 1). The steady-state fluorescence spectra of **HNO** at room temperature also show single K* emission in *n*-hexane and dual emission in methanol and acetonitrile (Fig. 1). The somewhat structured K* band in *n*-hexane, with a shoulder at 510 nm, is characteristic of the naphthoxazole moiety.[17] This emission band becomes structureless but does not undergo significant spectral shift in going from hydrocarbon to more polar solvents (Table 1). Unlike this almost solvent polarity-independent K* fluorescence, E* emission exhibits a perceptible change from 415 nm in acetonitrile to 430 nm in methanol (Fig. 1). This behaviour agrees with an E* form with a strongly separated electronic charge in S_1 and with a K* form in which polarization is compensated with the proton translocation.[18] In **HBO** and **HPO** this effect is logically less pronounced, as they undergo a smaller change in polarization of the enol tautomer upon excitation. Notably, the K* emission wavelength in hydrocarbon solvents slightly changes when going from **HPO** (480 nm in methylcyclohexane[16]) to **HBO** (500 nm in *n*-hexane[8d]) to **HNO** (493 nm in *n*-hexane). In contrast to the observed by Nagaoka[10] and Ijima[12] for naphtha- and anthra-derivatives of **HBO**, our results suggest that benzannulation at the oxazole moiety exerts little impact on proton-transfer emission.

Vertical transitions energies

Computational modeling of the vertical $S_0 \rightarrow S_1$ transition using time-dependent density functional theory (TDDFT) for **HPO**, **HBO** and **HNO** at B3LYP/6-31+G(d) level in acetonitrile predicted energies of 4.02 eV (308 nm), 3.77 eV (329 nm) and 3.41 eV (363 nm), respectively. Despite the fact that vertical energies are used in most of the benchmarks to compare with the experimental λ_{max} and, in addition, some authors recommend their use,[19,20] it should be noted that these values are vibrationless difference between S_0 and S_1.[21] This implies an extra approximation that could introduce an additional error added to the errors inherent to the functional and the solvent model. However, these values are useful to rationalize the changes between different compounds and different solvents. According to DFT calculation, the HOMO → LUMO transition is the dominant contributor to the first singlet excited state of the three compounds (see ESI† for MOs depiction). The computed HOMO–LUMO gap energies are close to the excitation energies of the three molecules in acetonitrile. Elongation of π-system decreases the HOMO–LUMO gap mainly due to LUMO stabilization (Fig. 2), which is related to the red shift in absorption observed in going from **HPO** to **HNO**.

Table 2 Theoretical emission maxima and oscillator strength (*f*, in parentheses) calculated at B3LYP/6-31+G(d) level of theory in acetonitrile

	$\lambda_{emission}$ (nm), *f*	
Compound	Enol S_1	Keto S_1
HPO	355 (0.659)	443 (0.312)
HBO	384 (1.049)	464 (0.452)
HNO	433 (0.811)	483 (0.579)

For fluorescence, the vertical $S_1 \rightarrow S_0$ energies at the S_1 geometries were calculated for the enol and keto forms of the three compounds in acetonitrile employing the linear response model of PCM (LR-PCM). B3LYP/6-31+G(d) predicts energies that are in close agreement with experimental data, even without accounting for vibrational effects (Table 2). Other

Table 3 Evaluation of different DFT functionals in reproducing the emission energies of **HNO**. Basis set employed: 6-31+G(d). Solvent model: LR-PCM

		$\lambda_{emission}$ (nm)				
	Solvent[a]	B3LYP	CAM-B3LYP	M06-2X	PBE0	ωB97XD
Enol S_1	Cyc	418	361	360	397	356
	DCM	429	378	377	409	372
	MeCN	433	383	382	414	377
	MeOH	433	383	381	414	377
Keto S_1	Cyc	497	424	429	471	421
	DCM	485	429	434	464	427
	MeCN	483	431	436	463	429
	MeOH	483	431	436	463	429

[a] Cyc, DCM, MeCN and MeOH stand for cyclohexane, dichloromethane, acetonitrile, and methanol, respectively.

popular functionals lead to considerable deviations, as it is shown in Table 3 for **HNO**. In general, all the tested DFT functionals predict blue-shifted emissions if compared with B3LYP, for either enol or keto isomers. Hybrid functionals B3LYP and PBE0 give the values closest to the experimental energies, whereas the meta-hybrid GGA functional M06-2X, the range-separated functional CAM-B3LYP and the dispersion-corrected functional ωB97XD overestimate the emission energies, giving rise to similar outcomes. This behaviour seems to be typical of these functionals in predicting fluorescence energies and it has been already observed in other similar ESIPT-based systems.[22] Furthermore, the use of non-equilibrium solvation models such as corrected linear response PCM (cLR-PCM) and state specific PCM (SS-PCM) does not improve the performance of the different functionals, but rather the opposite. Overall, the mean unsigned error (MUE) values for the fluorescence energies of the enol and keto forms of **HNO** were 0.19 and 0.26 eV, respectively, with the LR-PCM model, 0.48–0.42 eV with cLR-PCM and 0.50–0.44 eV using SS-PCM (Tables S1 and S2 in ESI†). In a previous work,[23] even more refined solvent models had to be used to improve the accuracy of the modelling to ESIPT dyes.

Effect of benzannulation on the $S_0 \rightarrow S_1$ excitation character

As it can be seen in Fig. 2 for **HPO**, molecular orbital distribution shows a HOMO mainly localized in the phenolic unit and a LUMO distributed over the heterocyclic part. This suggest that the HOMO → LUMO transition implies a considerable redistribution of electron density, as evidenced by the decrease of the contribution from the OH group to the molecular orbital and the increase of the N-acceptor contribution in oxazole in going from HOMO to LUMO. This is an important feature, since electron redistribution plays a major role in ESIPT mechanism as it sets the stage for the subsequent proton transfer.[18]

In order to shed light on the nature of this process, the charge transfer (CT) character at the geometry of the E* minimum of each molecule was qualitatively examined through TDDFT calculations. The change on electron density upon excitation calculated with B3LYP/6-31+G(d) in acetonitrile is showed in Fig. 3 (top). In **HPO**, a visible change of density takes place on the OH group (blue lobe) together with an increase of electron density above the N atom (red lobe) in going from S_0 to S_1. The electron flux is mostly directed from phenol towards the heterocyclic part of the molecule, making the N atom more basic and thus favouring the subsequent proton transfer. In the case of **HBO**, the electron density redistribution is similar to that of **HPO**, although slightly less pronounced. This situation changes dramatically for **HNO**, as the $S_0 \rightarrow S_1$ transition causes a strong polarization and thus exhibits a more marked CT character. It is important to note that the OH group of **HNO** plays a rather marginal role in the redistribution of electron density, in contrast to the cases of **HPO** and **HBO**. The unusual charge transfer character observed for **HNO** is closely related to the incorporation of an electron-rich benzene ring to the heterocyclic part of the molecule.

The electrostatic potential maps depicted in Fig. 3 (bottom) help to clarify the CT involved in the excitation to the S_1 state of

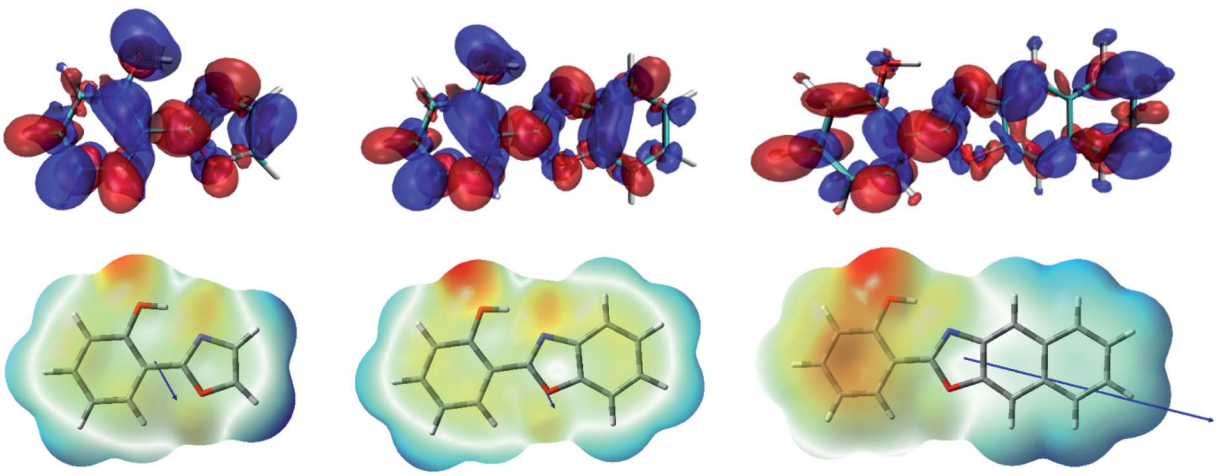

Fig. 3 Top: density difference plots ($\Delta\rho = \rho_{S_1} - \rho_{S_0}$, isovalue = 0.0004) calculated with B3LYP/6-31+G(d) in acetonitrile. The blue/red zones indicate a decrease/increase of electron density upon excitation, respectively. Bottom: electrostatic potential maps and dipole moment vectors for the three compounds in acetonitrile.

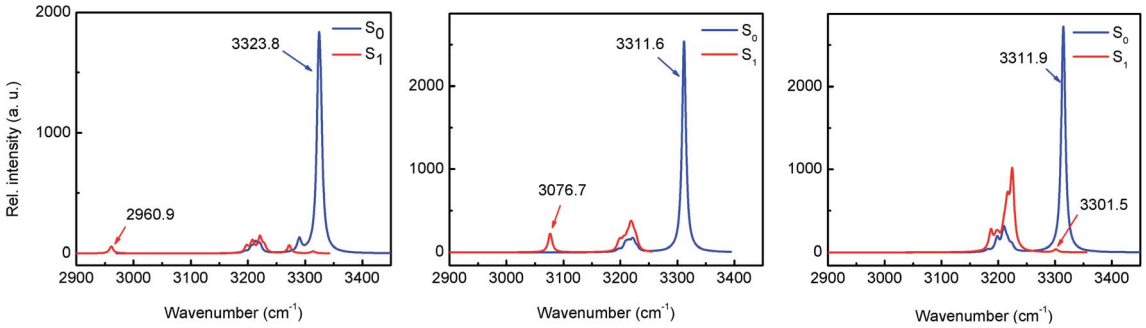

Fig. 4 IR spectra of **HPO** (left), **HBO** (middle) and **HNO** (right) in the S_0 and S_1 states calculated with B3LYP/6-31+G(d) in acetonitrile depicting the red shifting of O–H stretching mode upon excitation.

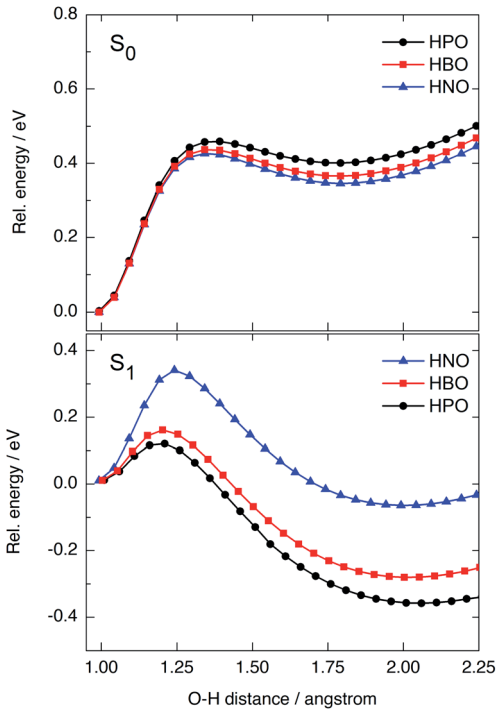

Fig. 5 PES calculated at B3LYP/6-31+G(d) level in acetonitrile for **HPO** (black), **HBO** (red) and **HNO** (blue) in the ground (top) and excited (bottom) states. For each curve, the energies are relative to the energy of the corresponding adiabatic enol minimum.

HNO. The large dipole moment of enol form in S_1 (10.4 D) reflects the considerable polarization that takes place according to B3LYP results. Due to this solute polarization, the ESIPT reaction could experience a certain solvent-polarity induced barrier, with the consequent separation between E* and K* forms along the reaction coordinate.[24] This effect is less likely to occur in **HPO** and **HBO**, since their dipole moments at the E* minimum in S_1 are considerably smaller (2.6 D and 3.0 D, respectively). The distinctive behaviour of **HNO** *versus* its lower analogues upon light absorption could have a strong influence on ESIPT reactivity, as it is demonstrated in the following sections.

Impact of benzannulation on the H-bond strength

The existence of an intramolecular H-bond between proton donor and acceptor sites is a prerequisite for ESIPT to occur.[5] For most ESIPT systems it is well known that such an interaction becomes stronger upon photoexcitation, which leads to an almost barrierless process. The strength of the H-bond can be estimated through the computation of the IR vibrational modes corresponding to the O–H bond (specifically, the O–H stretching frequency) in either ground or excited states.[25] The results of the computational calculations for the enol forms of **HPO**, **HBO** and **HNO** reveal different behaviours for each one of them (Fig. 4). In **HPO**, the O–H stretching is red-shifted by 363.8 cm^{-1} upon excitation, from 3323.8 cm^{-1} to 2960.9 cm^{-1}, which provides evidence for the O–H···N bond enhancement in S_1. In the case of **HBO** this effect is slightly smaller, with a red shift of 234.9 cm^{-1}. Surprisingly, in **HNO** the enhancement of H-bond in S_1 state is rather negligible, as the change in the O–H vibrational frequency in going from S_0 to S_1 is only 10.4 cm^{-1}. These results concur with those obtained from NCI (non-covalent interaction)[26] and QTAIM analysis[27,28] (see ESI for details†). The reason why the H-bond in **HPO**, **HBO** (and many other related systems[29]) becomes stronger in S_1 state owes to the fact that the electron density distribution over the N atom in S_1 is greater than in ground state, making that nitrogen more basic (Fig. 3). In contrast to these cases, in **HNO** the electron density moves away from N atom upon excitation due to the aforementioned larger extent of charge transfer. Therefore, in S_1 the N acceptor of **HNO** is at most as basic as in S_0, which should result in a similar proton-transfer reactivity in both electronic states. To confirm this hypothesis, it is necessary to model the potential energy surfaces in S_0 and S_1 states through DFT and TDDFT calculations, respectively.

Effect of the extension of oxazole π-conjugation on ESIPT reaction profile

We have modelled the ESIPT process for **HPO**, **HBO** and **HNO** using DFT and TDDFT computational calculations at the B3LYP/6-31+G(d)/IEFPCM level of theory. In ground state, the energy barrier for tautomerization (E → K) is quite high in all cases (0.42–0.46 eV, Fig. 5, top), which rules out the presence of the keto form in the S_0 state as one of the light-absorbing species at 298 K. The ground-state potential energy surface

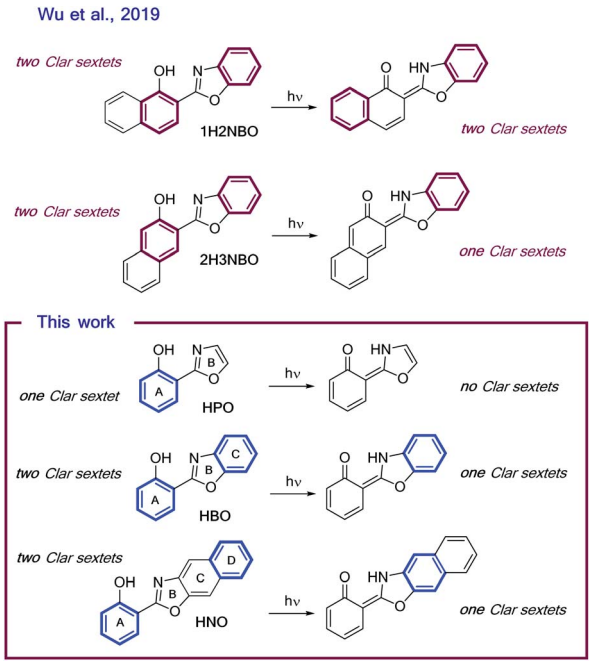

Fig. 6 Schematic illustrations of ESIPT in (A) **1H2NBO** and **2H3NBO** and (B) **HPO**, **HBO** and **HNO**. Clar's sextets are highlighted in bold.

(PES) of **HNO** (Fig. 5, top, in blue) lies at slightly lower energies than that of **HBO** (red) and **HPO** (black), indicating the S_0 K tautomer of **HNO** is somewhat more stable than the others. This makes sense if one considers that a naphthoxazole unit is richer in electrons than benzoxazole or oxazole moieties, and therefore it can accept a proton more easily. As there is a large energy difference between enol and keto forms in ground state, the back-proton transfer exhibits low barrier.

Vertical excitation of enol form to the Franck–Condon (FC) region of S_1 state is at 4.02 eV in **HPO**, 3.77 eV in **HBO** and 3.41 eV in **HNO** above ground-state PES (Fig. S9 in ESI†). The state decays to the local E* minimum on S_1 state, which lies almost ~0.25–0.27 eV below the FC level in the three cases. The energy barrier for proton transfer in S_1 increases with each successive benzannulation, from 0.11 eV (2.5 kcal mol^{-1}) in **HPO** to 0.16 eV (3.7 kcal mol^{-1}) in **HBO**, to 0.33 eV (7.6 kcal mol^{-1}) in **HNO** (Fig. 5, bottom). Note that for **HNO**, the proton transfer barrier in S_1 is comparable to that one in S_0 (0.42 eV) which can favour a radiative decay channel from E* to the ground state. Additionally, the K* tautomer of **HNO** is almost degenerate with the E* form, being the energy difference of only 0.08 eV (Fig. S9†), which implies a lower thermodynamic driving force for proton transfer.

Besides fluorescence emission, a possible deactivation channel from K* form in S_1 implies the adiabatic back-proton transfer to recover the E* tautomer on the S_1 PES by surmounting the reverse barrier. This barrier is estimated to be 0.50 eV for **HPO**, 0.46 eV for **HBO** and 0.40 for **HNO** at B3LYP/6-31+G(d) level in acetonitrile. As the K* form of **HNO** is higher in energy (relative to **HNO**-E*) than the K* form of the other dyes, it is easier for **HNO** to undergo back-proton transfer in excited state.

In summary, benzannulation of the oxazole core leads to higher energy barriers for ESIPT in the first singlet excited state and to a less stable K* tautomer, as a result of the modification of charge transfer properties. Nevertheless, the structural modification has little impact on ESIPT emission energies, unlike the observed for other benzazoles benzannulated at the phenol side.

Rationalization of the results under the light of Baird's rule

Recently, the "anomalous" emissive behaviour of the benzannulated **HBO** derivatives **1H2NBO** and **2H3NBO** (Fig. 6) was rationalized in terms of the Baird's rule.[13,14] Despite these compounds are structurally similar, they exhibit very different ESIPT emission with a maximum at 470 nm for **1H2NBO** and at

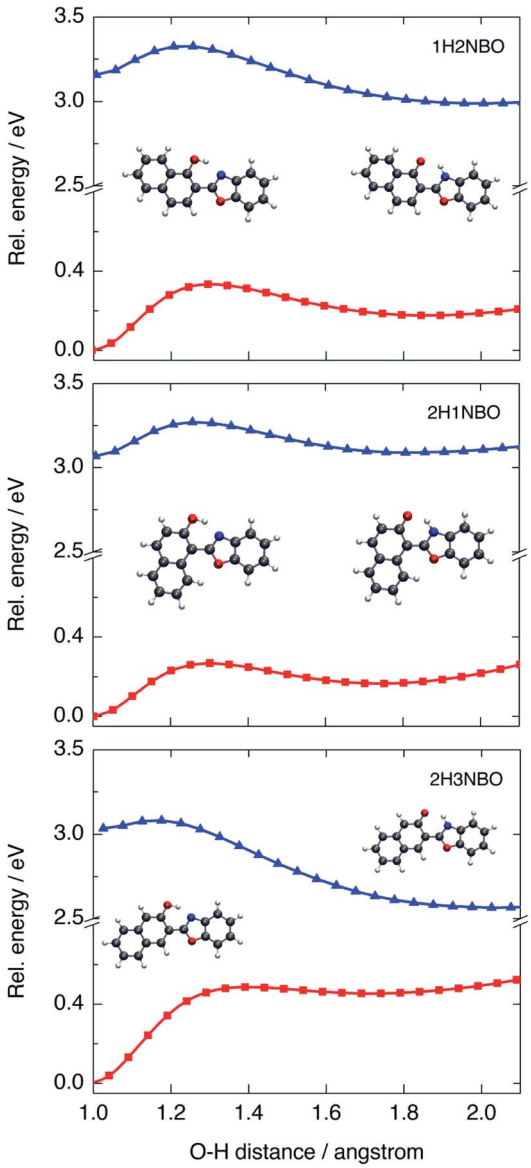

Fig. 7 PES calculated at B3LYP/6-31+G(d) level in acetonitrile for the three naphthol-derivatives **1H2NBO**, **2H1NBO** and **2H3NBO** in the S_0 (red) and S_1 (blue) states.

Table 4 NICS(1)$_{zz}$ values (in ppm) for enol and keto forms of **HPO**, **HBO** and **HNO** in the S_0 and S_1 states[a]

	S_0		S_1	
Dye		Global ΔNICS(1)$_{zz}$[b]		Global ΔNICS(1)$_{zz}$
HPO				
Enol	**−44.6** (−21.6, −23.0)	**0**	**29.1** (36.9, −7.8)	**73.7**
Keto	**−31.5** (−13.4, −18.2)	**13.1**	**10.7** (16.6, −5.8)	**55.3**
HBO				
Enol	**−66.7** (−20.8, −18.1, −27.8)	**0**	**28.3** (26.3, 0.1, 1.8)	**95.0**
Keto	**−52.3** (−12.5, −13.1, −26.8)	**14.4**	**−5.3** (12.1, −2.6, −14.8)	**61.4**
HNO				
Enol	**−92.4** (−20.5, −15.5, −28.9, −27.5)	**0**	**48.7** (−3.9, 1.3, 34.3, 16.9)	**141.1**
Keto	**−75.9** (−11.3, −10.4, −26.6, −27.6)	**16.5**	**−19.8** (10.1, −4.3, −9.5, −16.1)	**72.6**

[a] NICS(1)$_{zz}$ values were calculated at PW91/IGLOIII level of theory from the geometries optimised at ωB97X-D/6-311+G(d,p) level. For each compound, the individual values for A–D rings (in parentheses) are informed from left to right. The more negative (positive) the value, the more aromatic (antiaromatic) the character. [b] Variation with respect to the NICS(1)$_{zz}$ value of the ground-state enol form, for each molecule.

670 nm in the case **2H3NBO**. Considering the Baird's rule, ESIPT provides a way to get rid of Baird antiaromaticity by transferring a proton in the S_1 state for these compounds. Thus, the emission maximum of K* form of **1H2NBO** and **2H3NBO** varies depending on the antiaromaticity of the K* species formed. By combining Baird's rule[15] with Clar's aromatic π-sextet rule,[30] Wu *et al.* suggested that the relaxation of K* to the hot ground state relieves more antiaromaticity in **1H2NBO** than in **2H3NBO**, as the latter is considerably less antiaromatic in S_1.[14] The enol form of **1H2NBO** in S_1 exhibits two complete antiaromatic Clar's sextets that remains unchanged upon tautomerization, whereas in **2H3NBO** the formation of the keto isomer implies the loss of one of those sextets (Fig. 6). As a consequence, the keto form of **2H3NBO** is less antiaromatic (*ergo* more stable) than the one of **1H2NBO** in S_1, and therefore its fluorescence emission results red-shifted.

On the other hand, a cursory look on the structures of **HPO**, **HBO** and **HNO** reveals that the excited-state stabilization of these fluorophores should proceed with similar extent, since ESIPT could alleviate the antiaromaticity of only one Clar's sextet in all cases (Fig. 6). To validate this intuitive hypothesis, it is necessary to provide a quantitative estimation of excited-state aromaticity. The evaluation of aromaticity can be done by using different structural,[31] energetic,[32] magnetic,[33] electronic[34] and reactivity-based[35] descriptors. In the present case we have chosen the dissected nucleus-independent chemical shifts, NICS(1)$_{zz}$, analysis in order to provide a comparison with the results of Wu *et al.* According to NICS(1)$_{zz}$ analysis, aromatic compounds are characterized by large, negative values due to magnetic shielding induced by the diatropic ring current. On the other hand, antiaromatic rings exhibit paratropic current, which causes deshielding at the ring and thus affords positive NICS(1)$_{zz}$ values.

In the ground state the NICS(1)$_{zz}$ analysis predicts that all the rings (A–D, Fig. 6) of the enol form of **HPO**, **HBO** and **HNO** are strongly aromatic. In **HPO**, both A–B rings are almost equally

Table 5 NICS(1)$_{zz}$ values (in ppm) for enol and keto forms of **1H2NBO**,[a] **2H3NBO**[a] and **2H1NBO**[b] in the S_0 and S_1 states

	S_0		S_1	
Dye		Global ΔNICS(1)$_{zz}$[c]		Global ΔNICS(1)$_{zz}$[c]
1H2NBO				
Enol	**−90.4** (−26.2, −19.4, −17.4, −27.4)	**0**	**30.8** (21.5, 35.9, −11.0, −15.6)	**121.2**
Keto	**−69.2** (−25.2, −7.3, −10.9, −25.8)	**21.2**	**2.0** (5.8, 12.3, −2.9, −13.2)	**92.4**
2H3NBO				
Enol	**−91.3** (−23.9, −22.3, −17.6, −27.5)	**0**	**57.1** (38.3, 56.8, −15.1, −22.8)	**148.4**
Keto	**−73.5** (−15.7, −16.7, −14.0, −27.1)	**17.8**	**−9.8** (−0.1, 16.5, −5.8, −20.4)	**81.5**
2H1NBO				
Enol	**−90.2** (−26.6, −18.3, −17.9, −27.4)	**0**	**16.0** (8.9, 29.1, −9.2, −12.9)	**106.2**
Keto	**−71.5** (−24.9, −8.1, −12.3, −26.3)	**18.7**	**6.6** (8.1, 14.2, −3.7, −12.0)	**96.8**

[a] Extracted from ref. 14. [b] Calculated at PW91/IGLOIII level of theory from the geometries optimised at ωB97X-D/6-311+G(d,p) level. [c] Variation with respect to the NICS(1)$_{zz}$ value of the ground-state enol form, for each molecule.

aromatic, whereas in **HBO** the C ring is the most aromatic one. Curiously, C is also the most aromatic ring in **HNO**.

Upon photoexcitation, the E* form becomes globally antiaromatic in all cases, with NICS(1)$_{zz}$ values of +29.1, +28.3 and +48.7 ppm for **HPO**, **HBO** and **HNO**, respectively. The A ring in **HPO** and **HBO** turns largely antiaromatic in S_1, as Baird's rule predicts. Interestingly, the A ring in **HNO** remains slightly aromatic in S_1, whereas C and D rings exhibit considerable paratropicity. The relief of antiaromaticity, which is believed to stabilize the K* form, occurs mainly from the A ring in **HPO** and **HBO** but from the C and D rings in **HNO**. This results demonstrate, again, that **HNO** behaves differently than its lower analogues in excited state.

To determine the origin of the particular fluctuation of aromaticity observed in the ESIPT of **HNO**, the NICS(1)$_{zz}$ analysis was performed to the naphthol-containing derivatives **1H2NBO**, **2H3NBO**[9,14] and **2H1NBO**[12,13] (Scheme 2 and Fig. 7). Since the three compounds have the same number of rings than **HNO**, the comparison becomes straightforward. The resulting values are listed in Table 5.

The global NICS(1)$_{zz}$ value for the ground-state E tautomer is around −90 ppm in all cases, and *ca.* −70 ppm for the K form. However, this trend changes significantly upon excitation. At the E* geometry, **2H3NBO** is markedly more antiaromatic than **1H2NBO** and **2H1NBO** by 26.3 ppm and 41.1 ppm, respectively. The origin of this difference seems to be related with the paratropicity of the naphthol subunit: in **2H3NBO**, the local NICS(1)$_{zz}$ value of naphthol is 95.1 ppm, whereas in **1H2NBO** and **2H1NBO** is 57.4 and 38 ppm, respectively. This is a noteworthy aspect: while the Baird's rule predicts the naphthol system to be antiaromatic in the first singlet excited state (as suggested by Lampkin *et al.* using naphthalene as model[13]), the degree of antiaromaticity appears to be strongly dependent on the orientation of naphthol with respect to the rest of the molecule in the studied examples. As a consequence, it is difficult to explain why the **2H3NBO** derivative becomes more antiaromatic than the others on the sole basis of this rule.

Computed ΔNICS(1)$_{zz}$ (K*–K) for **2H3NBO** (Δ = 63.7 ppm), **1H2NBO** (Δ = 71.2 ppm) and **2H1NBO** (Δ = 78.1 ppm) could give an idea of the relief of antiaromaticity that accompanies fluorescence emission (670 nm, 460 nm and 470 nm in hexane, respectively), as Wu *et al.* proposed.[14] However, there seems to be no lineal relationship between calculated ΔNICS(1)$_{zz}$ and fluorescence energy in a strict way. **1H2NBO** relieves more antiaromaticity than **2H3NBO** (*ca.* +7.5 ppm) in going from K* to K and its fluorescence emission is shorter than the one of **2H3NBO** by 200 nm. At the same time, **2H1NBO** relieves more antiaromaticity than **1H2NBO** (+6.9 ppm), but the fluorescence maxima of both compounds are very close among each other (460 *vs.* 470 nm). So, a similar relief of antiaromaticity is associated with a huge red shift in emission in one case but not in another. To fully understand this discrepancy, it is necessary to go beyond Baird's rule and consider the ESIPT process further.

The PES modelled at the S_0 and S_1 states for the proton-transfer process in **1H2NBO**, **2H1NBO** and **2H3NBO** are shown in Fig. 7. **1H2NBO** and **2H1NBO** exhibit similar energetic profiles, although they differ in that TDDFT predicts the ESIPT reaction of **1H2NBO** to be endergonic by *ca.* 0.02 eV. Lampkin *et al.* attributed this endergonicity to an error associated with the geometry optimization of K*,[13] but it seems rather to be a typical feature of the ESIPT compounds in which an extra fused ring is located at a non-favourable position.[36] Furthermore, in some cases CASSCF calculations also predicts endergonic ESIPT, in the same way as TDDFT does.[37] In any case, it is undeniable that ESIPT in **2H3NBO** is far more exothermic than in the other cases. This behaviour is consistent with the results of NICS(1)$_{zz}$ analysis. The large stabilization of K* in **2H3NBO** can be interpreted as a result of the considerable relief of antiaromaticity associated with the E* → K* photoisomerization (ΔNICS(1)$_{zz}$ = 66.9 ppm), much larger than that of **1H2NBO** (28.8 ppm) and **2H1NBO** (10 ppm). As can be seen in Fig. 7, the red-shifted emission of **2H3NBO** is a consequence of the proximity of both the S_1 and the S_0 surfaces. The high energy of the K form in ground state can be understood in terms of the Clar's rule, since its formation implies the loss of one aromatic Clar's sextet. Unlike this case, the K tautomer in **1H2NBO** and **2H1NBO** preserves the Clar's sextet of the naphthol system after isomerization, which makes it logically more stable in S_0 and leads to a larger S_0–S_1 energy gap. These observations are a clear example of the complementarity between Baird's and Clar's rules applied to ESIPT.

Finally, we can compare the results of the NICS(1)$_{zz}$ analysis in order to provide a complete description of the effect of benzannulation on ESIPT in terms of excited state aromaticity. If we compare the local changes in aromaticity that take place during ESIPT, the behaviour of **HNO** results very different to that of the naphthol-containing dyes **1H2NBO**, **2H1NBO** and **2H3NBO**. While in this series the naphthol subunit becomes antiaromatic upon light absorption, in **HNO** the rise of antiaromaticity occurs at the heterocyclic part of the molecule. Moreover, the phenol ring in the E* form of **HNO** does not exhibit paratropicity at all in the S_1 state, despite being a Clar's sextet that should be antiaromatic according to the Baird's rule. The same applies for the benzoxazole moiety of **1H2NBO**, **2H1NBO** and **2H3NBO**, which never becomes locally antiaromatic in S_1. In summary: the fluctuation pattern of excited state aromaticity in **HNO** appears to be the opposite of that in the naphthol-containing series.

One possible explanation for this odd behaviour is that charge transfer in S_1 can actually modulate the aromaticity of different regions within the same molecule. As we have detailed before in this text, in **HNO** the vertical transition to the first singlet excited state exhibits a considerable CT character which increases the electron density of the phenol ring. This increment is connected with the small but negative NICS(1)$_{zz}$ value of that ring in the E* form of **HNO** (−3.9 ppm, Table 4), which seems to indicate that CT avoids the ring to become antiaromatic. At the same time, π depletion of C–D rings of **HNO** makes them markedly antiaromatic in S_1. This trend is reverted as ESIPT occurs, since it implies the translocation of a proton and an electron towards the heterocyclic moiety (see Fig. S11 in ESI†). At the K* geometry, the CT direction has been reverted and the C–D systems are no longer antiaromatic but, at the same time, the A ring has become antiaromatic in turn.

The same analysis can be applied for **2H3NBO**, which is the only dye of the naphthol series exhibiting a significant degree of CT in the S_1 state (see Fig. S12 in ESI†). As it was previously discussed, the E* tautomer of **2H3NBO** shows high paratropicity at the π-depleted naphthol unit and significant diatropicity at the rest of the molecule. Since the CT direction (naphthol-to-benzoxazole) does not change during ESIPT in **2H3NBO**, the aromatic character of benzoxazole remains almost unaltered during E* → K* isomerization. Within the series, the varying CT character finely tunes the aromaticity of the rings: the higher the electron density gained, the more aromatic the system and more stable the K* tautomer (compare Table 5 and Fig. S12†). This could explain both the deeply exothermic ESIPT in **2H3NBO** and also the endergonic one in **2H1NBO**.

From what precedes, charge transfer arises as an essential aspect that must be considered for a complete rationalization of the impact of benzannulation on ESIPT. In a more general sense, ESIPT can be facilitated by the combination of two effects: on the one hand, the antiaromaticity alleviation caused by CT in the S_1 state and on the other hand, the basicity enhancement of the proton-acceptor site caused by the electron redistribution. When light absorption triggers CT in an unfavourable direction (as in **HNO**), the subsequent ESIPT becomes hampered due to the lack of driving force.

In agreement with the reported by Wu *et al.*, ESIPT provides a way to avoid antiaromaticity in excited state, but mostly because of the effect of electron redistribution. The exact mechanism by which CT modulates the excited-state aromaticity/antiaromaticity of a ring is not fully understood at this stage, but further work could lead to a comprehensive knowledge of the phenomenon.

Conclusions

The results presented in this study demonstrated that the ESIPT reactivity is significantly affected by the size of the π-conjugated framework. Unlike previous cases, benzannulation at the heterocyclic part of **HPO** does not lead to a significant red shift in ESIPT emission. Moreover, benzannulation of **HBO** to give **HNO** causes a remarkable change in the charge transfer character of the $S_0 \rightarrow S_1$ excitation that leads to a redistribution of electron density from the naphthoxazole subunit to the phenol ring. As a consequence, there is a large barrier for ESIPT in the S_1 state. The extension of conjugation also decreases the basicity of the N acceptor and weakens the intramolecular O–H···N bond, essential for ESIPT to occur.

On the other hand, benzannulation of **HBO** at the phenol unit leads to a very large redshift in emission only when it occurs at a specific site of the molecule, as proposed by Nagaoka *et al.* This particular array allows to maximize the CT extent in the S_1 state.

The results presented herein can be interpreted using the Baird's rule and the Clar's rule of sextets. Nevertheless, the local variations of aromaticity observed for individual rings in the S_1 state cannot be explained satisfactorily by using these approaches only. The analysis of local $NICS(1)_{zz}$ fluctuation during the ESIPT process becomes meaningful when the CT character of the S_1 state is considered. This observation seems to suggest that CT in S_1 is actually able to alleviate the local Baird antiaromaticity in ESIPT compounds, providing a driving force for the process. The impact of CT on the excited-state aromaticity requires detailed theoretical and experimental work, which will be the focus of future work.

Materials and methods

All reagents and solvents were obtained from Sigma Aldrich and used as received. Spectroscopic grade solvents were used for UV-vis absorption and fluorescence spectra measurements. UV-visible spectra of the compounds in solution were recorded with a Shimadzu UV-1800 Spectrophotometer at 25 °C. Fluorescence spectra of the samples were recorded with an Agilent Cary Eclipse Fluorescence Spectrophotometer at 25 °C. ^{1}H NMR and ^{13}C NMR were recorded on a 400 MHz Bruker nuclear magnetic resonance spectrometer.

Synthesis

HNO was synthesized according to a reported protocol,[38] by reaction of 355 mg (2.2 mmol) of 3-amine-2-naphthol with 370 mg (2.7 mmol) of salicylic acid in 10 mL of polyphosphoric acid. The reaction mixture was heated to 180 °C for 3 h and then poured into ice water and neutralized with $NaHCO_3$. The solid was filtered, washed with water and purified by column chromatography using hexane/ethyl acetate 100 : 0 to 80 : 20 as eluent.

2-(Naphtho[2,3-*d*]oxazol-2-yl)phenol (HNO).[38] White solid. Yield: 28%. ^{1}H NMR (400 MHz, ($CDCl_3$, 25 °C)): δ 11.58 (s, 1H), 8.16 (s, 1H), 8.09 (dd, J = 7.9, 1.4 Hz, 1H), 7.94–8.04 (m, 3H), 7.56–7.45 (m, 3H), 7.15 (d, J = 8.3 Hz, 1H), 7.04 (t, J = 7.5 Hz, 1H) ppm. ^{13}C NMR (101 MHz, $CDCl_3$) δ 165.1, 159.6, 148.2, 140.0, 134.3, 131.9, 131.8, 128.6, 128.1, 127.8, 125.9, 125.2, 119.8, 117.7, 116.7, 110.5, 106.7 ppm.

Computational methods

All DFT and TDDFT calculations were performed using the Gaussian 09 program.[39] The relevant stationary points were fully optimized using the B3LYP functional with the 6-31+G(d) basis set, although CAM-B3LYP, M06-2X, PBE0 and ωB97XD functionals were also used in certain cases for comparative purposes. The nature of the obtained stationary points was verified by Hessian diagonalization and harmonic frequency analyses. Solvent effects were included using three different formalisms: linear response PCM (LR-PCM), corrected linear response PCM (cLR-PCM) and state specific PCM (SS-PCM) with non-equilibrium solvation. Relaxed scans were computed by allowing all the internal degrees of freedom to relax apart from the driving coordinate (O–H distance, step length = 0.05 Å). Vertical excitation and emission energies were calculated within the linear response scheme of TDDFT. For NCI and QTAIM analyses the Multiwfn software was used.[40] The dissected nucleus-independent chemical shifts ($NICS(1)_{zz}$) were calculated at 1 Å above the different rings taking into account only contributions from the out-of-plane tensor component

perpendicular to the ring planes. NICS(1)$_{zz}$ values were computed using the PW91 functional with the IGLOIII basis set. For the estimation of NICS(1)$_{zz}$ in the S_1 state, NICS calculations were performed as open-shell triplet states employing the geometries optimized at the S_1 state as reported by Wu *et al.*[14] Visualization and graphics rendering were carried out with GaussView 5.0.8 (ref. 41) and VMD 1.9.3.[42]

Conflicts of interest

There are no conflicts to declare.

Acknowledgements

This work was partly supported by Consejo Nacional de Investigaciones Científicas y Técnicas (CONICET), Secretaría de Ciencia y Tecnología, Universidad Nacional de Córdoba (SECyT), and Agencia Nacional de Promoción Científica y Técnica (ANPCyT). We thank Lucas J. Karas for his generous help with NICS(1)$_{zz}$ calculations. L. D. M. gratefully acknowledges the fellowship granted from CONICET.

References

1 C. Yang, J. Zhang and W. Peng, *Sci. Rep.*, 2018, **8**, 16359.
2 C.-T. Chen, *Chem. Mater.*, 2004, **16**, 4389–4400.
3 J. P. Celli, B. Q. Spring, I. Rizvi, C. L. Evans, K. S. Samkoe, S. Verma, B. W. Pogue and T. Hasan, *Chem. Rev.*, 2010, **110**, 2795–2838.
4 (*a*) P. Coppo, M. Duati, V. N. Kozhevnikov and L. Hofstraat, *Angew. Chem., Int. Ed.*, 2005, **44**, 1806–1810; (*b*) Y. J. Yang, M. Lowry, C. M. Schowalter, S. O. Fakayode, J. O. Escobedo, X. Y. Xu, H. T. Zhang, T. J. Jensen, F. R. Fronczek, I. M. Warner and R. M. Strongin, *J. Am. Chem. Soc.*, 2006, **128**, 14081–14092; (*c*) P. Zhou and K. Han, *Acc. Chem. Res.*, 2018, **51**, 1681–1690.
5 V. S. Padalkar and S. Seki, *Chem. Soc. Rev.*, 2016, **45**, 169–202.
6 (*a*) H. Zollinger, *Color Chemistry*, WileyVCH, Zurich, 3rd edn, 2001, p. 550J; (*b*) E. Kwon and S. Y. Park, *Adv. Mater.*, 2011, **23**, 3615–3642.
7 Y. Yamaguchi, Y. Matsubara, T. Ochi, T. Wakamiya and Z. Yoshida, *J. Am. Chem. Soc.*, 2008, **130**(42), 13867–13869.
8 (*a*) L. Lavtchieva, V. Enchev and Z. Smedarchina, *J. Phys. Chem.*, 1993, **97**, 306–310; (*b*) O. K. Aboud-Zied, *Chem. Phys.*, 2007, **337**, 1–10; (*c*) A. Fernández-Ramos, J. Rodríguez-Otero, M. A. Ríos and J. Soto, *J. Mol. Struct.*, 1999, **489**, 255–262; (*d*) O. K. Abou-Zied, R. Jimenez, E. H. Z. Thompson, D. P. Millar and F. E. Romesberg, *J. Phys. Chem. A*, 2002, **106**, 3665–3672; (*e*) T. Arthen-Engeland, T. Bultmann, N. P. Ernsting, M. A. Rodríguez and W. Thiel, *Chem. Phys.*, 1992, **163**, 43–53; (*f*) M. Krishnamurthy and S. Dogra, *J. Photochem.*, 1986, **32**, 235–242; (*g*) V. S. Padalkar, P. Ramasami and N. Sekar, *J. Lumin.*, 2014, **146**, 527–538; (*h*) S. Lochbrunner, K. Stock and E. Riedle, *J. Mol. Struct.*, 2004, **700**, 13–18; (*i*) Z. Yuan, Q. Tang, K. Sreenath, J. T. Simmons, A. H. Younes, D. Jiang and L. Zhu, *Photochem. Photobiol.*, 2015, **91**, 586–598.
9 S.-I. Nagaoka, J. Kusunoki, T. Fujibuchi, S. Hatakenaka, K. Mukai and U. Nagashima, *J. Photochem. Photobiol., A*, 1999, **122**, 151–159.
10 S.-I. Nagaoka and U. Nagashima, *J. Phys. Chem.*, 1990, **94**, 1425–1431.
11 T. Kanda, A. Momotake, Y. Shinohara, T. Sato, Y. Nishimura and T. Arai, *Bull. Chem. Soc. Jpn.*, 2009, **82**, 118–120.
12 T. Iijima, A. Momotake, Y. Shinohara, T. Sato, Y. Nishimura and T. Arai, *J. Phys. Chem. A*, 2010, **114**, 1603–1609.
13 B. J. Lampkin, Y. H. Nguyen, P. B. Karadakov and B. VanVeller, *Phys. Chem. Chem. Phys.*, 2019, **21**, 11608–11614.
14 C.-H. Wu, L. J. Karas, H. Ottosson and J. I.-C. Wu, *Proc. Natl. Acad. Sci. U. S. A.*, 2019, **116**, 20303–20308.
15 N. C. Baird, *J. Am. Chem. Soc.*, 1972, **94**, 4941–4948.
16 D. LeGourriérec, V. Kharlanov, R. G. Brown and W. Rettig, *J. Photochem. Photobiol., A*, 2000, **130**, 101–111.
17 A. Ghodbane, J. Colléaux, N. Saffon, R. Mahiou, J.-P. Galaup and S. Fery-Forgues, *ChemPlusChem*, 2013, **78**, 185–191.
18 C.-C. Hsieh, C.-M. Jiang and P.-T. Chou, *Acc. Chem. Res.*, 2010, **43**, 1364–1374.
19 A. Painelli and F. Terenziani, *Chem. Phys. Lett.*, 1999, **312**, 211–220.
20 G. E. Jara, C. A. Solis, N. S. Gsponer, J. J. Torres, C. A. Glusko, C. M. Previtali, A. B. Pierini, D. M. A. Vera, C. A. Chesta and H. A. Montejano, *Dyes Pigm.*, 2015, **112**, 341–351.
21 A. D. Laurent, C. Adamo and D. Jacquemin, *Phys. Chem. Chem. Phys.*, 2014, **16**, 14334–14356.
22 (*a*) D. Jacquemin, A. Planchat, C. Adamo and B. Mennucci, *J. Chem. Theory Comput.*, 2012, **8**, 2359–2372; (*b*) C. Azarias, Š. Budzák, A. D. Laurent, G. Ulrich and D. Jacquemin, *Chem. Sci.*, 2016, **7**, 3763–3774.
23 P. M. Vérité, C. A. Guido and D. Jacquemin, *Phys. Chem. Chem. Phys.*, 2019, **21**, 2307–2317.
24 A. Demchenko, K.-C. Tang and P.-T. Chou, *Chem. Soc. Rev.*, 2013, **42**, 1379–1408.
25 G. J. Zhao and K.-L. Han, *J. Phys. Chem. A*, 2007, **111**, 2469–2474.
26 J. Contreras-García, R. Boto, F. Izquierdo-Ruiz, I. Reva, T. Woller and M. Alonso, *Theoretical Chemistry Accounts: Theory, Computation, and Modeling*, Springer Verlag, 2016, vol. 135, p. 242.
27 R. F. W. Bader, *Chem. Rev.*, 1991, **91**, 893–928.
28 R. F. W. Bader, *Atoms in Molecules - A Quantum Theory, International Series of Monographs on Chemistry*, Oxford University Press, Oxford, 1990, vol. 22.
29 (*a*) J. Zhao, H. Dong, H. Yang and Y. Zheng, *Org. Chem. Front.*, 2018, **5**, 2710–2718; (*b*) Y. Yang, H. Zhai, Y. Liu, X. Jia, Y. He, Q. Ma, K. Jiang and Y. Liu, *J. Lumin.*, 2019, **216**, 116736.
30 E. Clar, *The Aromatic Sextet*, Wiley, London, NY, 1972.
31 T. M. Krygowski, H. Szatylowicz, O. A. Stasyuk, J. Dominikowska and M. Palusiak, *Chem. Rev.*, 2014, **114**(12), 6383–6422.
32 M. K. Cyrański, *Chem. Rev.*, 2005, **105**, 3773–3811.
33 R. H. Mitchell, *Chem. Rev.*, 2001, **101**, 1301–1315.

34 F. Feixas, E. Matito, J. Poater and M. Solà, *Chem. Soc. Rev.*, 2015, **44**, 6434–6451.
35 Z. Mucsi, B. Viskolcz and I. G. Csizmadia, *J. Phys. Chem. A*, 2007, **111**, 1123–1132.
36 (*a*) K.-C. Tang, M.-J. Chang, T.-Y. Lin, H.-A. Pan, T.-C. Fang, K.-Y. Chen, W.-Y. Hung, Y.-H. Hsu and P.-T. Chou, *J. Am. Chem. Soc.*, 2011, **133**, 17738–17745; (*b*) J. Piechowska and G. Angulo, *Dyes Pigm.*, 2019, **165**, 346–353; (*c*) S. Prasad De, S. Ash, S. Dalai and A. Misra, *THEOCHEM*, 2007, **807**, 33–41; (*d*) N. Zhang, T. Zhang, L. Wen, L. Wang, J. Yan and K. Zheng, *Phys. Chem. Chem. Phys.*, 2020, **22**, 1409–1415.
37 W. Yang and X. Chen, *Phys. Chem. Chem. Phys.*, 2014, **16**, 4242–4250, principio del formulario.
38 N. A. Padilla, M. T. Rea, M. Foy, S. P. Upadhyay, K. A. Desrochers, T. Derus, K. A. Knapper, N. H. Hunter, S. Wood, D. A. Hinton, A. C. Cavell, A. G. Masias and R. H. Goldsmith, *ACS Sens.*, 2017, **2**, 903–908.
39 M. J. Frisch, G. W. Trucks, H. B. Schlegel, G. E. Scuseria, M. A. Robb, J. R. Cheeseman, G. Scalmani, V. Barone, B. Mennucci, G. A. Petersson, H. Nakatsuji, M. Caricato, X. Li, H. P. Hratchian, A. F. Izmaylov, J. Bloino, G. Zheng, J. L. Sonnenberg, M. Hada, M. Ehara, K. Toyota, R. Fukuda, J. Hasegawa, M. Ishida, T. Nakajima, Y. Honda, O. Kitao, H. Nakai, T. Vreven, J. A. Montgomery Jr, J. E. Peralta, F. Ogliaro, M. Bearpark, J. J. Heyd, E. Brothers, K. N. Kudin, V. N. Staroverov, R. Kobayashi, J. Normand, K. Raghavachari, A. Rendell, J. C. Burant, S. S. Iyengar, J. Tomasi, M. Cossi, N. Rega, J. M. Millam, M. Klene, J. E. Knox, J. B. Cross, V. Bakken, C. Adamo, J. Jaramillo, R. Gomperts, R. E. Stratmann, O. Yazyev, A. J. Austin, R. Cammi, C. Pomelli, J. W. Ochterski, R. L. Martin, K. Morokuma, V. G. Zakrzewski, G. A. Voth, P. Salvador, J. J. Dannenberg, S. Dapprich, A. D. Daniels, Ö. Farkas, J. B. Foresman, J. V. Ortiz, J. Cioslowski and D. J. Fox, *Gaussian 09, Revision E.01*, Gaussian, Inc., Wallingford CT, 2009.
40 T. Lu and F. Chen, *J. Comput. Chem.*, 2012, **33**, 580–592.
41 R. Dennington, T. Keith and J. Millam, *GaussView, Version 5*, Semichem Inc., Shawnee, Mission, KS, 2009.
42 *Visual Molecular Dynamics (VMD), version 1.9.3*, http://www.ks.uiuc.edu/Research/vmd.